

# The angular two-point correlation of NVSS galaxies revisited

Song Chen<sup>\*</sup> and Dominik J. Schwarz<sup>\*\*</sup>

Fakultät für Physik, Universität Bielefeld, Postfach 100131, 33501 Bielefeld, Germany

Preprint online version: July 8th, 2015

## ABSTRACT

We measure the angular two-point correlation and angular power spectrum from the NRAO VLA Sky Survey (NVSS) of radio galaxies. Contrary to previous claims in the literature, we show that it is consistent with primordial Gaussianity on all angular scales and it is consistent with the best-fit cosmological model from the Planck analysis, as well as the redshift distribution obtained from the Combined EIS-NVSS Survey Of Radio Sources (CENSORS). Our analysis is based on an optimal estimation of the two-point correlation function and makes use of a new mask, which takes into account direction dependent effects of the observations, side lobe effects of bright sources and galactic foreground. We also use a lower flux threshold and take the cosmic radio dipole into account. The latter turns out to be an essential step in the analysis. This improved cosmological analysis of the NVSS stresses the importance of a flux calibration that is robust and stable on large angular scales for future radio continuum surveys.

**Key words.** Radio galaxy, NVSS mask, Primordial Non-Gaussianity

## 1. Introduction

Continuum radio galaxy surveys can probe large cosmic volumes. The mean redshift of observed radio galaxies is significantly larger than the mean redshift of modern optical surveys. Optical surveys allow us to obtain photometric or even spectroscopic redshift measurements, which is not the case for continuum radio galaxy surveys. Nevertheless, the information contained in continuum radio galaxy surveys can be useful to probe cosmological models. An example is the investigation of non-Gaussianity via angular two-point correlations. In this work we revisit some aspects of the cosmological analysis of continuum radio galaxy surveys.

Most of our current understanding of cosmology relies on observations of the cosmic microwave background (CMB). Planck satellite data extended our understanding to the high multipole CMB, they allowed us to successfully measure the cross-correlation between the large scale structure and the CMB through the integrated Sachs-Wolfe (ISW) and lensing effects. In the study of the ISW effect, large-scale radio continuum catalogs play an important role. For the Planck analysis the NRAO VLA Sky Survey (NVSS) (Condon et al. 1998) has been utilized (Planck Collaboration. XIX. 2014).

Radio galaxy surveys, such as the NVSS, have large sky coverage and extend to redshifts well beyond unity. Their angular two-point correlation function and angular power spectrum are useful probes of large scale cosmology. With new radio continuum surveys, containing between 10 million to a few billions of objects, such as from the Low Frequency Array (LOFAR)<sup>1</sup>, the Australian Square Kilometre Array Pathfinder (ASKAP)<sup>2</sup>, the South African MeerKAT radio telescope (MeerKAT)<sup>3</sup> or the

Square Kilometre Array (SKA)<sup>4</sup>, more complete and precise radio point source catalogues will be available. These surveys will allow us to probe several interesting aspects of cosmology, for a recent review see Jarvis et al. (2015). Among them accurate investigations of the largest cosmic structures.

For cosmological analysis the fundamental observable from a surveys is the surface density of sources above a given flux density limit, i.e. the integral of the differential number count per solid angle per flux density interval, as a function of position on the sky. A study that includes all effects of the surface density at linear order in cosmological perturbation theory has been presented recently (Maartens et al. 2013; Chen & Schwarz 2015). These could be modified by local effects of large structures, e.g. by local voids (Rubart et al. 2014). Radio continuum surveys are also a good candidate to further test several CMB anomalies (Schwarz et al. 2004; Naselsky et al. 2012; Copi et al. 2015; Yoho et al. 2015; Planck Collaboration. XVI 2015).

Previously, Blake & Wall (2002b) explored the angular two-point correlation of the NVSS catalogue at small angular separation ( $\theta < 10^\circ$ ). Besides, they also measured the angular power spectrum of the same catalogue (Blake et al. 2004), and found that their result seems to be incompatible with a high redshift population of radio galaxies. Xia et al. (2010) suggested that the clustering at  $1^\circ \leq \theta \leq 8^\circ$  is dominated by some non-Gaussian component. They quote the non-Gaussianity parameter  $f_{\text{nl}} = 62 \pm 27$ . Hernández-Monteagudo (2010) investigated in detail the two-point cross correlation between the NVSS catalogue and the CMB temperature anisotropies from the Wilkinson Microwave Anisotropy Probe (WMAP) in angular and multipole space. He did not find any evidence for the cross correlation in the range  $l \in [2, 10]$ , where according to the simulation 50% of the signal is expected. He concluded that the large scale clustering excess, he found in the NVSS catalogue, is unlikely to be caused by contaminants or systematics, since it appears to be independent of the flux density threshold.

<sup>\*</sup> e-mail: songchen at physik.uni-bielefeld.de

<sup>\*\*</sup> e-mail: dschwarz at physik.uni-bielefeld.de

<sup>1</sup> URL: www.lofar.org

<sup>2</sup> URL: www.atnf.csiro.au/projects/askap/

<sup>3</sup> URL: http://www.ska.ac.za/meerkat/

<sup>4</sup> URL: www.skatelescope.org

In this work, we explore the full range of the angular two-point correlation function ( $0^\circ < \theta < 180^\circ$ ) with a focus on large angular scales ( $\geq 1^\circ$ ), and compare it with the flat  $\Lambda$  cold dark matter ( $\Lambda$ CDM) model. All previous analyses are based on masking of the galaxy by a constant latitude cut. Moreover the cosmic radio dipole (Ellis & Baldwin 1984; Blake & Wall 2002a) has not been accounted for in previous works. To extract the auto-correlation signal from the catalog in a reliable way, we propose a more sophisticated NVSS mask and subtract the a cosmic radio dipole. Based on side lobe contamination estimates and noise properties of the NVSS catalogue, we provide a mask that leaves us with a sky coverage of 64.7% at a minimal specific flux density of 15 mJy.

Our work is structured as follows. In section 2 we review the properties NVSS catalog and explain our masking method. In section 3, we review the theoretical angular two-point correlation function based on the  $\Lambda$ CDM model. We present the angular two-point correlation obtained by means of the Landy-Szalay estimator using our mask in section 4. In section 5 we discuss our results, followed by a conclusion (section 6).

## 2. The NVSS catalogue

The NRAO VLA Sky Survey Condon et al. (1998) used the D and DnC antenna configurations of the Very Large Array (VLA). The survey was carried out between 1993 and 1997. Continuum intensity and linear polarization images at 1.4 GHz have been obtained, covering the whole northern and part of the southern sky at declinations  $\delta > -40^\circ$ . The D configuration of the VLA was used to cover the sky from  $\delta = -10^\circ$  to  $\delta = 78^\circ$ , the rest was filled in by means of the DnC configuration. The obtained images have on average FWHM resolution  $\theta_{\text{FWHM}} = 45''$ , which is significantly larger than the median angular size of faint extragalactic sources (around  $10''$ ). This survey design sacrifices resolution to achieve high surface brightness, which is needed to achieve flux-limit completeness.

Since the NVSS point-source response is much larger than the median angular size of extragalactic sources, most of the information on the NVSS total intensity images is well represented by elliptical Gaussian fits. The fitted parameters formed the NVSS catalog of sources (not all of them are individual sources). The NVSS catalogue contains almost 2 million discrete sources with flux density above 2.5 mJy. Below we use the source positions in right ascension  $\alpha$  and declination  $\delta$ , the integrated flux density  $S$ , as well as their errors.

The NVSS catalogue contains several artificial effects (Ho et al. 2008): First, the catalogue shows a configuration effect, which is easily seen in figure 1 as steps in surface density at  $\delta \sim 78^\circ$  and  $\delta \sim -10^\circ$ , which are the borders between the D and DnC configurations on the map. Secondly, the side lobes of the bright sources can obscure the presence of weak nearby sources. They are not completely removed by cleaning. The NVSS local dynamic range of the total intensity images is about 1000 to one. Thus, sources closer than about  $0.6^\circ$  to a bright source of flux density  $S$  and fainter than  $10^{-3}S$  may only be caused by side lobes (Condon et al. 1998).

Besides these two unphysical effects, there is also a foreground of point sources mainly from the Milky Way (see figure 1) and smooth components of radiation from the galaxy itself. These contaminations can influence the VLA noise temperature, and further change the completeness in certain areas on the sky.

All these effects need to be treated carefully, otherwise the statistical analysis based on the contaminated map will be bi-

$S >$	5 mJy	10 mJy	15 mJy	25 mJy
$\chi^2$	160.1	59.7	30.7	21.5

**Table 1.**  $\chi^2$ -values testing for the isotropy in declination of the NVSS surface density (here with 13 degrees of freedom).

ased. Here we choose to apply a lower flux density threshold and to mask the catalogue to address these issues.

### 2.1. Lower flux density threshold

Two different VLA configurations (D and DnC) have been used to compile the NVSS catalogue. The VLA C configuration is less compact and thus has a better resolution of  $15''$ , compared to  $45''$  of the D configuration. The DnC configuration is a hybrid configuration in which the antennas on the east and west arms are in D configuration, but those on the north arm are in C configuration to enhance their view of sources at low elevation. Using the DnC configuration changes the synthesized beam and the resolution of declination with respect to the D configuration. This shifts the brightness sensitivity and completeness between the parts of sky observed with different configurations.

The source catalog is derived from intensity images, therefore it is brightness sensitivity limited. Apparently, the D configuration has higher brightness sensitivity than the DnC configuration. Thus one expects to obtain a more complete catalogue for the part of the sky observed by means of the D configuration.

The completeness shift of the DnC configuration sky w.r.t. the D configuration sky can be considered as a faint source selection based on the position angle, noise, confusion and cataloging procedures. It is not clear whether this selection may further introduce a tension in source distribution between the two parts of the sky. Therefore, it is safe to either use one configuration alone (which would reduce the sky coverage by an significant amount), or to choose a higher flux density threshold for the cosmological analysis (which reduces the source density and increases the shot noise).

Blake & Wall (2002b) argue that this configuration effect is only significant at flux densities  $S < 10$  mJy. In figure 2 we plot the surface density fluctuation,  $\Delta\sigma/\bar{\sigma} = \sigma/\bar{\sigma} - 1$ , as a function of declination. The dependence of the surface density fluctuation on declination resembles the theoretical rms noise level of the NVSS catalogue (Condon et al. 1998), which is further discussed below in section 5. One can see that the declination dependence of the surface density is less than 2.5% and the mean value of the DnC configuration is clearly lower than that of the D configuration. This configuration effect is more pronounced at lower thresholds.

This finding is also supported by a  $\chi^2$ -analysis testing for deviations from isotropy in declination

$$\chi^2 \equiv \sum_{i=1}^{N_{\text{bin}}} \frac{\left(\frac{\Delta\sigma_i}{\bar{\sigma}}\right)^2}{\left(\delta\left[\frac{\Delta\sigma}{\bar{\sigma}}\right]_i\right)^2} = \sum_{i=1}^{N_{\text{bin}}} \Omega_i \frac{(\Delta\sigma_i)^2}{\sigma_i}, \quad (1)$$

where  $\Omega_i$  denotes the solid angle of the  $i$ th declination strip. The results of this test are shown in table 1.

In this work, we choose flux density thresholds of 15 mJy and 25 mJy for cosmological analysis for following the reasons: The study of the the configuration effect suggests that there is a significant dependence on declination. As it is shown above, a flux density threshold of 15 mJy or 25 mJy reduces the value of  $\chi^2$  dramatically compared to the situation with lower thresholds.

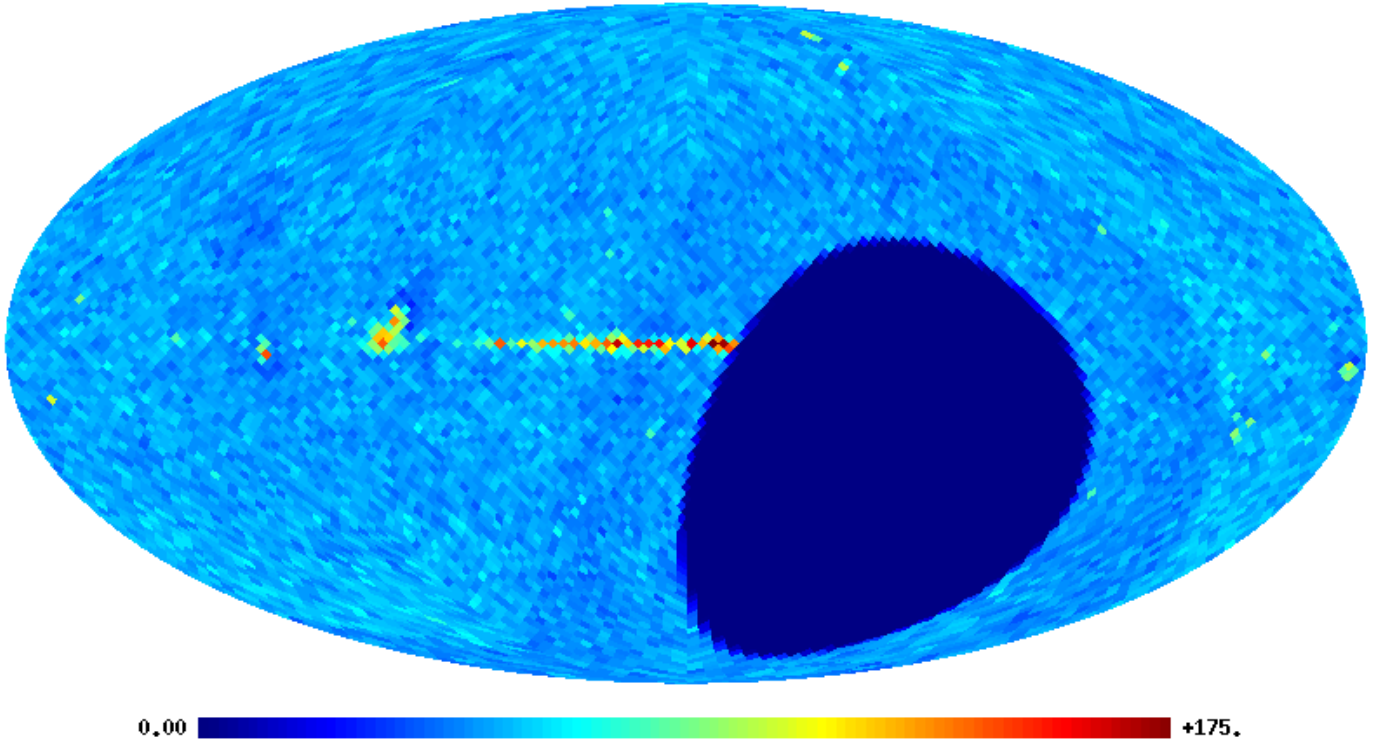


**Fig. 1.** Surface density of the NVSS source catalog in galactic coordinates in Mollweide projection, shown at HEALPIX resolution  $N_{\text{side}} = 32$ . The color bar shows the surface density in units of number of objects per square degree. Here we include all objects contained in the catalogue.

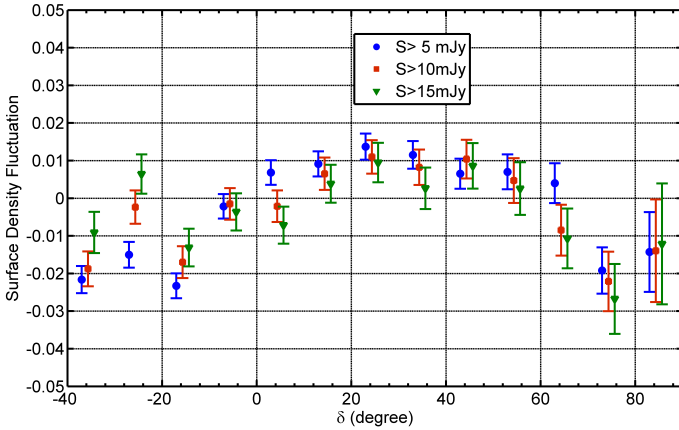


**Fig. 2.** Surface density fluctuation,  $\Delta\sigma/\bar{\sigma}$ , of the NVSS catalogue as a function of declination for several flux density thresholds. The error bars assume Poisson distributed source counts and we mask the region  $|b| \leq 5^\circ$ . For clarity, the horizontal positions of the  $S > 5$  mJy and  $S > 15$  mJy data points are slightly offset.

As we do not expect a perfect agreement with isotropy, it is not justified to rise the threshold even higher.

Our choice is supported by studies of the cosmic radio dipole from NVSS, which is one to two orders of magnitudes larger than the higher multipole moments. The previous NVSS dipole measurements show that for thresholds below 15 mJy, the dipole direction differs significantly from the CMB dipole direction, and the reduced  $\chi^2$  of the quadratic dipole estimator increases significantly (Blake & Wall 2002a; Gibelyou & Huterer 2012; Rubart & Schwarz 2013; Rubart 2015).

No cut-off at high flux densities is introduced as there is only a small number of sources at high flux densities and thus they

play a subdominant role only. We also expect them to be less affected by calibration systematics.

## 2.2. Masking strategy

Nevertheless, we have to mask regions around the brightest sources in order to minimize contamination from their side lobes. In the analysis of Ho et al. (2008) all sources above 2.5 Jy have been masked by a disk with a radius of  $0.6^\circ$ . However, not all side lobes appear as spurious entries in the catalog, a uniform masking strategy will erase all the information from bright sources, since all sources above the cut threshold are masked. In Blake & Wall (2002b) a list of 22 masks around bright galaxies was compiled based on a visual inspection of the survey.

Here, we introduce an automatic bright source selection method. We count the number of nearby (within  $0.6^\circ$ ) sources with  $S > 15$  mJy of the brightest sources whose flux densities are  $S > 2.5$  Jy. The corresponding histogram is shown in Fig. 3.

We assume that the number of sources in a fixed solid angle follows a Poisson distribution, and use the so-called Poissonness plot (Hoaglin & Tukey 2006) to identify the histogram bins that are significantly deviate from a Poisson distribution, where we assume that such a deviation is caused by the side lobe contamination of bright sources. The idea of the plot is to consider a simple variable substitution, which transforms the exponential Poisson distribution function to a linear function. We find that 49 sources fail the Poissonness test at the 99% confidence level (Fig. 4). It is worth clarifying that ‘clean’ regions containing bright sources that by chance contain the same amount of sources as ‘dirty’ regions are also excluded. We also verify that for most of the bright sources the nearby source count histogram is in good agreement with the histogram of randomly picked

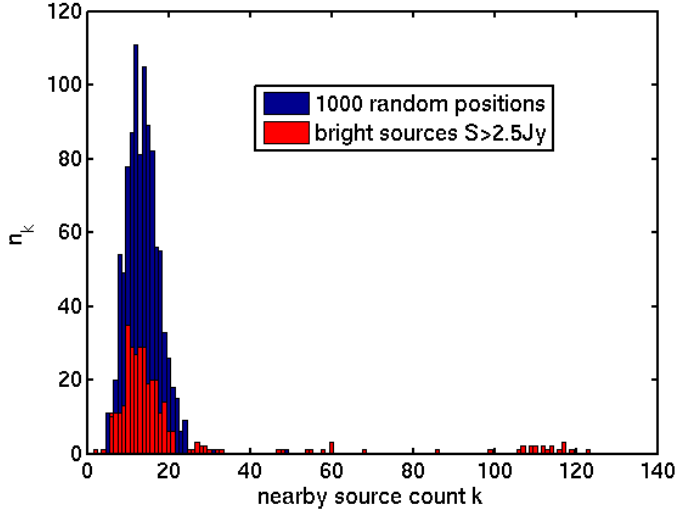


**Fig. 3.** Nearby source count histogram (disks with radius  $0.6^\circ$ ). The red bins correspond to nearby source counts around bright radio galaxies with  $S > 2.5$  Jy. The blue bins correspond to 1000 randomly picked positions outside the galactic plane ( $|b| > 5^\circ$ ). The maximum of randomly picked counts results in 49 nearby sources.

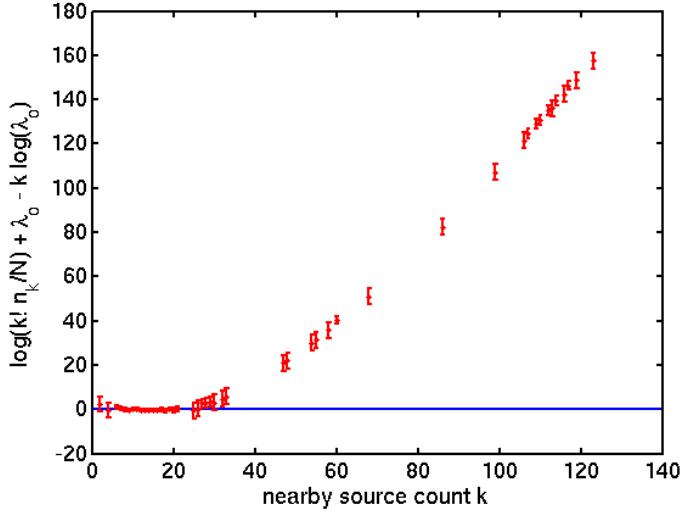


**Fig. 4.** Poissonness plot of the nearby source counts.  $\lambda_0$  is the mean nearby count over the survey area.  $N$  is the total number of sources with  $S > 2.5$  Jy. The solid horizontal line corresponds to a perfectly Poisson distributed nearby source count. The error bars denote the 99% confidence levels.

nearby source counts, which justifies the inclusion of many of the bright sources in our analysis.

Let us now turn to the issue of noise and confusion. According to Condon et al. (1998), the rms position uncertainty  $\sigma_{\text{pos}}$  is,

$$\sigma_{\text{pos}} \propto \frac{\sigma_b \theta_{\text{FWHM}}}{2S_p}, \quad (2)$$

where  $S_p$  is the peak flux density,  $\sigma_b$  is the rms brightness fluctuation (noise and confusion). Our idea is to use  $\sigma_p$  to trace  $\sigma_b$ . Condon et al. (1998) point out that for flux densities below 15 mJy, the rms position uncertainty is dominated by noise. Accordingly, we create a position uncertainty map (Fig. 5) by

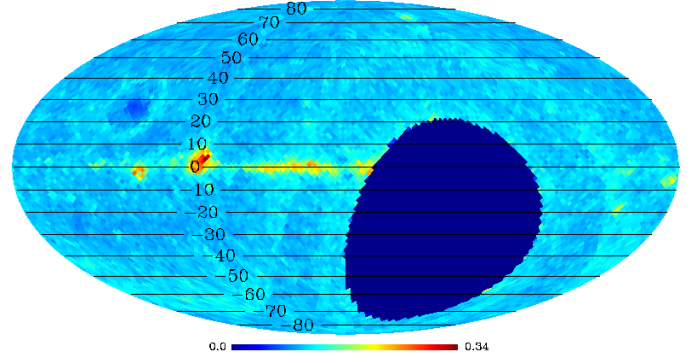


**Fig. 5.** NVSS position uncertainty map, relative to the mean beam width  $\theta_{\text{FWHM}} = 45''$ .

averaging the position uncertainties

$$\sigma_\theta \equiv \sqrt{\frac{\sigma_\delta \sigma_\alpha}{\theta_{\text{FWHM}}^2} \sin\left(\frac{\pi}{2} - \delta\right)} \quad (3)$$

for all point sources in a pixel whose flux density is smaller than 15 mJy. Note that the dominant sources are those with low flux density. The map is constructed using the HEALPIX package with the pixel size fixed by  $N_{\text{side}} = 32$ .

The resulting position uncertainty map is shown in Fig. 5. One sees clearly that the position uncertainty follows the theoretical rms noise level which, outside of the galactic plane, increases away from the zenith due to pickup of ground radiation, atmospheric emission, ionospheric effects and uv-projection. The galactic plane and nearby nebulas are also easy to identify. We further employ a 5% pixel cutoff for the pixels with highest  $\sigma_\theta > 0.132$ . In addition, we also mask galactic radio sources by excluding all sources with galactic latitude  $|b| \leq 5^\circ$ .

To sum up, at 15 mJy and 25 mJy thresholds we mask all pixels in the neighborhood of 49 selected bright sources. Additional pixels and their neighborhood with highest mean position uncertainty  $\sigma_\Omega$  and galactic sources with  $|b| \leq 5^\circ$  are masked as well. In the following we call this the NVSS65 mask<sup>5</sup>. It is shown in Fig. 6. In total, there is approximately 64.7% sky left. The total number of objects after applying the NVSS65 mask at 15 and 25 mJy is shown in Table 3.

### 3. Angular two-point correlation: theoretical expectation

The angular two point correlation function  $w(\theta)$  is a powerful tool to measure the projected large-scale structure distribution of the Universe. It is defined as the joint probability  $\delta P$  of finding galaxies in both of the elements of solid angle  $\delta\Omega_1$  and  $\delta\Omega_2$  separated by an angle  $\theta$  (Peebles 1980),

$$\delta P = \bar{\sigma}^2 \delta\Omega_1 \delta\Omega_2 [1 + w(\theta)]. \quad (4)$$

At linear order, the full relativistic expression of the surface density of sources above flux density  $S_t$  is (Chen & Schwarz

<sup>5</sup> At the moment the NVSS65 mask is available at <https://github.com/phychemsong/NVSS>.

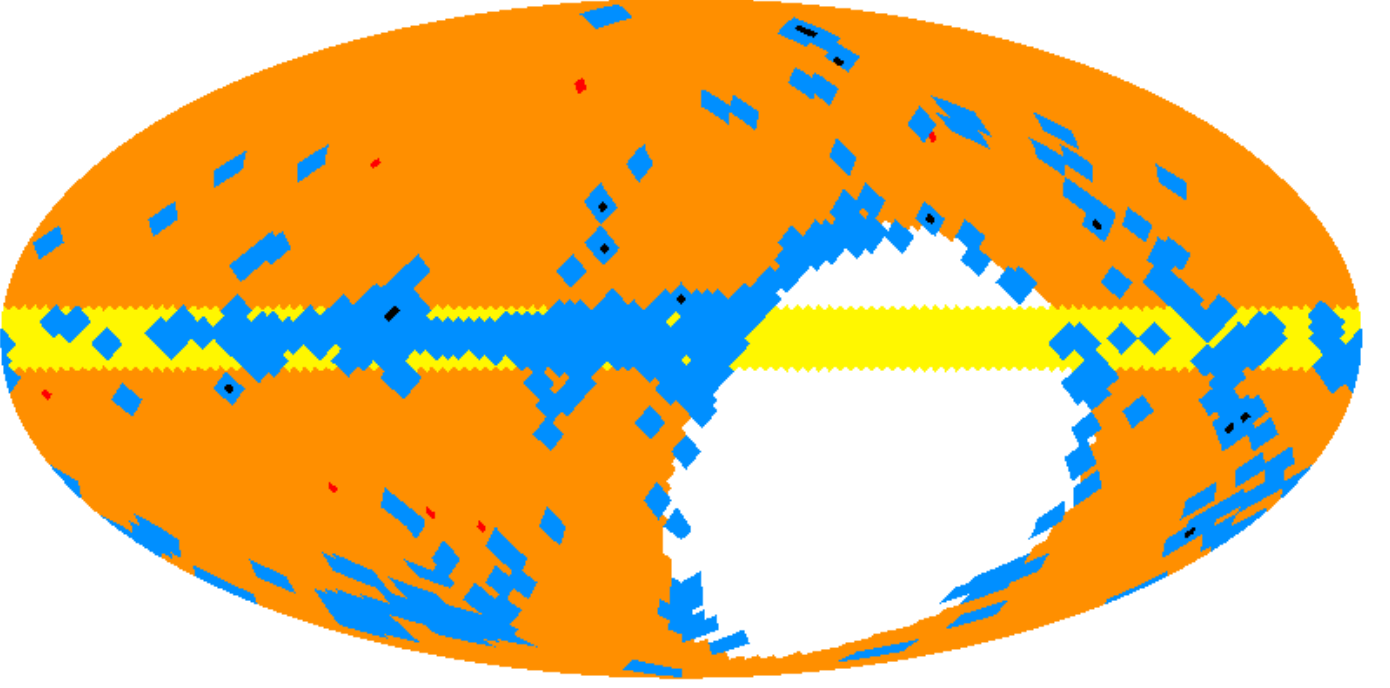


**Fig. 6.** NVSS65 mask. The orange region makes up 64.7% of the sky. Yellow pixels are close to the galactic plane  $|b| \leq 5^\circ$  and are excluded to suppress galactic point sources and foregrounds. Blue pixels are excluded due to large position errors. Red and black pixels contain bright sources with significant side lobe effects, black pixels additionally overlap with pixels with high position error.

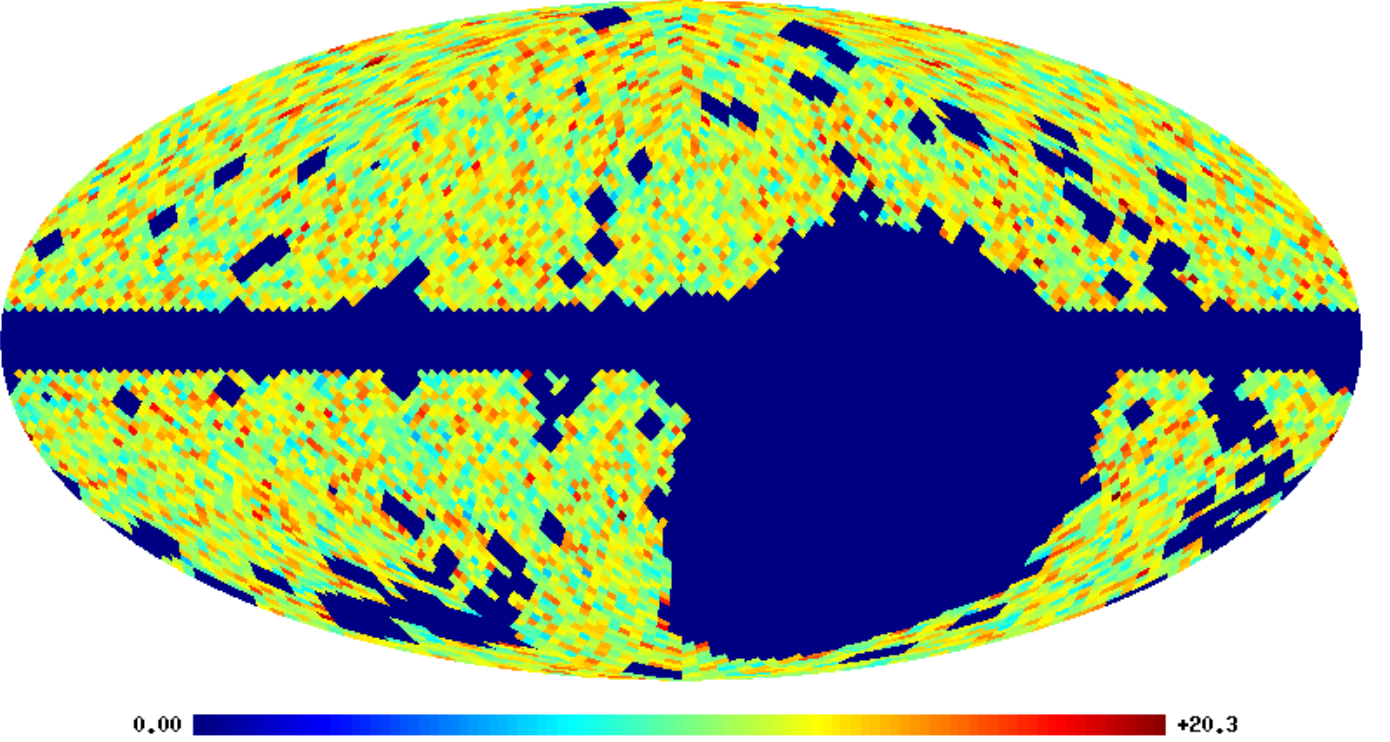


**Fig. 7.** Surface density of the NVSS source catalog for a flux density threshold of  $S > 15$  mJy and applying the NVSS65 mask, shown in galactic coordinates at pixel size  $N_{\text{side}}=32$ . The color bar shows the surface density  $\sigma$  in units of number of objects per square degree.

2015),

$$\sigma(> S_i) = \int_{S_i}^{\infty} \frac{dS_o}{S_o} \frac{a^3 r_o^3 \bar{n}_{\text{phy}}}{2 + (\bar{a} + 1) r_o \mathcal{H}} [1 + \delta_n + 3\psi + \Delta E + V^i e_i^r + 2 \frac{\delta r}{r_o} + \frac{\partial \delta r}{\partial r_o} - 2\kappa_g], \quad (5)$$

where,  $S_o$  is the observed flux density,  $a$  is the scale factor,  $r_o$  is the inferred comoving distance,  $\bar{a}$  is the mean source spectrum index,  $\mathcal{H}$  is the conformal Hubble parameter, and  $\bar{n}_{\text{phy}}$  is the physical mean number density. Inside the brackets, the most important contribution comes from the number density fluctua-



tion  $\delta_n$ . The other terms describe volume distortion via the scalar metric perturbations  $\psi$  and  $E$ , light cone projection involving the projected source velocity  $V^i e_i^r$ , radial distance fluctuation  $2\delta r/r_0 + \partial\delta r/\partial r_0$ , which lead to a fluctuations of flux density, and lensing convergence  $\kappa_g$ . We only take the dominant leading term, i.e. physical number density fluctuation, into account, and neglect all other effects. This is justified since the statistical and systematic fluctuations from the NVSS catalogue are well above the expected size of the sub-leading linear effects.

The luminosity and density evolution of radio galaxies is significant. Therefore, we turn to redshift space,

$$\begin{aligned}\sigma(> S_l) &\approx c \int dz \frac{a^3 r_0^2}{H} \bar{n}_{\text{phy}} [1 + \delta_n] \\ &= \int dz \frac{d\bar{\sigma}}{dz} [1 + b\delta],\end{aligned}\quad (6)$$

where  $b = b(z)$  denotes the bias of radio galaxies and  $\delta$  is the matter density contrast in synchronous comoving coordinates.

We use the Combined EIS-NVSS Survey Of Radio Sources (CENSORS) (Brookes et al. 2008) to model the redshift distribution of the NVSS catalogue. CENSORS contains all NVSS sources above 7.2 mJy that are within a patch of  $6 \text{ deg}^2$  in the ESO Imaging Survey (EIS). Following Marcos-Caballero et al. (2013), we choose the gamma function redshift distribution,

$$\frac{d\bar{\sigma}}{dz} = \mathcal{N} \left( \frac{z}{z_0} \right)^\beta \exp \left( -\beta \frac{z}{z_0} \right), \quad (7)$$

with  $\mathcal{N}$  denoting a normalization factor that is irrelevant for the final result and the best-fit parameters to CENSORS data given by  $z_0 = 0.53_{-0.13}^{+0.11}$  and  $\beta = 0.81_{-0.32}^{+0.34}$ . These numbers should however be treated with care as the redshift distribution is based on 149 galaxies only.

Due to the broad shape of the luminosity function, the radio galaxy redshift distribution shows only a weak dependence of the flux threshold (de Zotti et al. 2010; Blake et al. 2004). This argument holds true, as for  $S > \text{few mJy}$  the differential number counts are dominated by active galactic nuclei, i.e. the flux density threshold is well above the flux density of a typical star forming galaxy.

For a statistically isotropic distribution of radio galaxies the angular two-point correlation  $w(\theta)$  can be determined from the angular power spectrum  $C_l$ ,

$$w(\theta) = \frac{1}{4\pi} \sum_l (2l+1) C_l P_l(\cos \theta), \quad (8)$$

where  $P_l(x)$  are Legendre polynomials. The angular power spectrum  $C_l$  of the surface density fluctuation can be calculated from the underlying matter power spectrum,

$$C_l = 4\pi \int_0^\infty \frac{dk}{k} P(k) T(k)^2 f(l, k)^2, \quad (9)$$

with  $P(k)$  denoting the primordial power spectrum of density fluctuations,  $T(k)$  the matter transfer function and

$$f(l, k) = \int \frac{d\bar{\sigma}}{dz} b(z) j_l[ck\eta(z)] D(z) dz, \quad (10)$$

where  $(d\bar{\sigma}/dz)$  is the differential number density of sources at flux density above  $S_l$ ,  $b(z)$  denotes the bias,  $j_l(x)$  is a spherical Bessel function of first kind,  $\eta = \eta(z)$  denotes conformal time, and  $D(z)$  is the growth factor.

For the galaxy bias, we use the second-order polynomial from the Planck 2015 analysis of the integrated Sachs-Wolfe effect (Planck Collaboration. XXI. 2015), which is an approximation of the Gaussian bias evolution model of Xia et al. (2010),

$$b(z) = 0.9 \left[ 1 + 0.54(1+z)^2 \right]. \quad (11)$$

For Non-Gaussianity bias see (Matarrese et al. 2000; Dalal et al. 2008). Finally, the expected  $C_l$  for the NVSS catalog are obtained using a modified version of the CLASS package (Di Dio et al. 2013).

The parameters for the best-fit cosmological model are taken from Planck Collaboration. XVI. (2014). For the theoretical prediction of the angular two-point correlation we cut the Legendre series at  $l_{\text{max}} = 900$ . We convinced ourselves that this cut-off is large enough to ensure numerical convergence of  $w(\theta)$  at all angular scales considered in this work.

## 4. Angular two-point correlation of radio galaxies

### 4.1. Optimal estimation

The angular two-point correlation could be estimated from (Peebles 1980)

$$1 + w(\theta) = \frac{DD}{N(N+1)/2} \frac{\Omega}{\langle \delta\Omega \rangle}, \quad (12)$$

where  $DD$  denotes the count of pairs at separation  $\theta$  and  $N$  denotes the total number of objects considered in the analysis. Thus  $N(N+1)/2$  is the total number of possible pairs.  $\Omega$  is the solid angle of the survey, and  $\langle \delta\Omega \rangle$  is the averaged solid angle of the ring  $\theta$  to  $\theta + \delta\theta$  within  $\Omega$  for a randomly placed ring center in  $\Omega$ .

For our analysis we use the optimal estimator found by Landy & Szalay (1993),

$$w_{\text{LS}}(\theta) = \frac{N_r(N_r+1)}{N(N+1)} \frac{DD}{\overline{RR}} - N(N_r+1) \frac{\overline{DR}}{\overline{RR}} + 1, \quad (13)$$

where  $\overline{RR}$  means the averaged pair count over a number of large random simulations, and  $\overline{DR}$  is the averaged data-random cross pair count for a number of large random simulations.  $N_r$  denotes the number of sources in the random catalogues. It is necessary to clarify that the simulated random sources  $R$  have to be identical for  $\overline{RR}$  and  $\overline{DR}$  to minimize the statistical uncertainty. Under the assumption that higher order correlations among galaxies can be ignored, the Landy-Szalay estimator has a ‘‘Poisson error’’

$$\delta w_{\text{LS}}(\theta) = \frac{1}{\sqrt{DD}} \frac{1 + w_{\text{LS}}(\theta)}{1 + w_\Omega}, \quad (14)$$

where  $w_\Omega$  is the mean of the two-point correlation function over the sampling geometry,

$$w_\Omega = \int_\Omega G_p(\theta) w(\theta) d\Omega \quad (15)$$

where  $G_p(\theta)$  is a dimensionless geometric form factor which is equal to the fraction of unique cell pairs separated by distance  $\theta \pm d\theta/2$  (Landy & Szalay 1993).

	$N$	$d$	$\alpha$	$\delta$
$S > 10$ mJy	436,733	$1.32 \times 10^{-2}$	$142.70^\circ$	$30.47^\circ$
$S > 15$ mJy	314,594	$1.44 \times 10^{-2}$	$153.44^\circ$	$-5.53^\circ$
$S > 25$ mJy	200,092	$1.83 \times 10^{-2}$	$157.12^\circ$	$-15.10^\circ$
expected		$0.46 \times 10^{-2}$	$168^\circ$	$-7^\circ$

**Table 2.** NVSS dipole for various flux density thresholds, measured by means of HEALPIX at resolution  $N_{\text{side}} = 32$  after applying the NVSS65 mask. For comparison we quote the expected kinetic dipole for NVSS radio sources, based on the observed CMB dipole.

#### 4.2. Dipole correction

The radio dipole signal is believed to result from our peculiar motion (Ellis & Baldwin 1984) with respect to the cosmic rest frame of radio galaxies, due to the fact that the mean redshift of radio galaxies is above one. If this rest frame is same as the CMB rest frame, then the dipole measured in the radio catalog should agree with the CMB dipole measured by WMAP and Planck (Jarosik et al. 2011; Planck Collaboration. XXVII. 2014). Previous studies (Blake & Wall 2002a; Singal 2011; Gibelyou & Huterer 2012; Rubart & Schwarz 2013) measured the radio dipole for the NVSS catalog. It is actually significantly larger than expected, by a factor of two to four, depending on the details of the analysis. The origin of this dipole excess is currently unknown. One possibility might be that it is a combination of local large-scale structure (Rubart et al. 2014) and a kinetic component due to Doppler shift and aberration.

A local structure dipole, as well as the kinetic dipole violate the assumption of statistical isotropy that is implicit in the way how we estimate  $w(\theta)$ . We suggest that the dipole signal needs to be taken into account, prior to the further correlation or power spectrum analysis. Indeed, also in our analysis the largest contribution to the angular two-point correlation of radio galaxies comes from the dipole moment of the galaxy distribution, as can be seen in Fig. 8. A significant effect can also be observed for the extracted multipole moments at low  $l$  (not shown here).

Utilizing HEALPIX, we find the radio dipole of the NVSS catalogue after masking with NVSS65 and as shown in table 2. The estimated dipole at our chosen flux density thresholds and sky coverage agrees with the estimates from the literature (see Rubart (2015) for a recent summary).

The standard dipole subtraction approach for pixelized maps is relative straightforward. First, one evaluates the dipole amplitude and direction through a linear dipole estimator on the pixelized map. Then one subtracts the measured dipole contribution at each pixel. However, we do not use the pixelized map to measure the correlation function, but rather extract it using the measured positions of all radio sources outside the mask. In order to do so, we have to include the effect of a dipole into the Landy-Szalay estimator.

Thus we simulate random catalogues with the measured dipole, denoted by  $R_d$  below, and employ the following estimator,

$$w_{\text{LS}}^d(\theta) = \frac{N_r(N_r + 1)}{N(N + 1)} \frac{DD}{RR} - N(N_r + 1) \frac{\overline{DR_d}}{RR} + \frac{\overline{R_d R_d}}{RR}. \quad (16)$$

The dipole simulations  $R_d$  are achieved by the following procedure. First, we assign a uniform random number  $t$  to each simulated object, then modify this number based on the angular separation  $\psi$  between the object and dipole direction,

$$t = \text{Random}[0, 1) + \frac{d}{2} \cos \psi \quad (17)$$

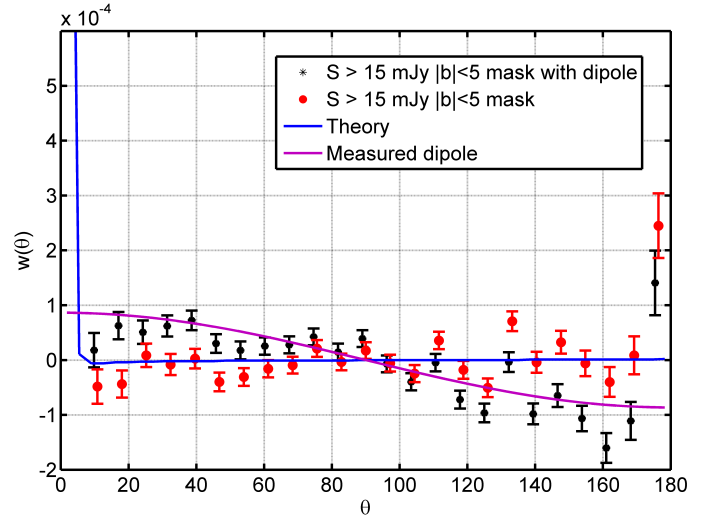


**Fig. 8.** NVSS angular two-point correlations for a  $5^\circ$  galactic latitude mask with and without dipole correction.

Then we add the objects with  $t \geq 0.5$  to the  $R_d$  catalogue and drop the others. Each random catalogue contains  $N_r = 10^6$  objects and we average over 10 such catalogues.

The dipole modified estimator (16) makes use of the full position information of the sources and by simulating several large random catalogues, we minimize the uncertainty in  $w_{\text{LS}}^d(\theta)$ . The computational load is a disadvantage of this procedure.

We can now compare the results without and with dipole subtraction. We either corrected for the measured radio dipole (see table 2) or for the CMB predicted radio dipole. The dipole contribution in the angular two-point correlation function can be seen from Fig. 8. We find that the dipole has a significant effect and actually dominates the two-point correlation function at large angular scales above  $\sim 10^\circ$ . In the figure we account for the measured dipole. Considering just the CMB predicted dipole reduces the large angle correlation, but leaves us with a residual dipole that could be due to a local structure and is hard to predict without a much more detailed study. We therefore decide to correct for the measured NVSS radio dipole and suppress the (structure) dipole also in the theoretical prediction.

#### 4.3. Results

We adopt the dipole subtracted Landy-Szalay estimator to measure the angular two-point correlations of the NVSS catalogue with thresholds 15 mJy and 25 mJy for two different masks (NVSS65 and a constant latitude cut of the galactic plane).

The results agree with our expectation. After masking of the high rms noise and confusion pixels by means of the NVSS65 mask, the two-point correlation turns out to be less scattered, as shown in Fig. 9. For the simpler constant latitude cut, one can see that the first data point at  $\sim 4^\circ$  is above the plot range of the figure. The NVSS65 mask efficiently reduces the amount of correlation at scales of a few degrees and brings the measurement in agreement with the theoretical expectation of the best-fit cosmological model. One can also observe a better agreement of the 15 and 25 mJy thresholded data sets after the mask NVSS65 has been applied. These findings are confirmed by the  $\chi^2$ -values shown in Table 3. We infer that the new NVSS65 mask efficiently pushes the data points towards the theoretical prediction.

One can also see from Fig. 9 that the measurement using the NVSS65 mask agrees with the theoretical prediction until

	$ b  < 5^\circ$		NVSS65	
	N	$\chi^2$	N	$\chi^2$
$S > 15$ mJy	377,739	165.96	322,557	94.08
$S > 25$ mJy	240,872	222.49	205,103	99.80

**Table 3.**  $\chi^2$ -test for  $w(\theta)$  for 49 data points [excluding first bin ( $0 < \theta < 3.6^\circ$ )]. Note: We neglect the correlation between the data points.

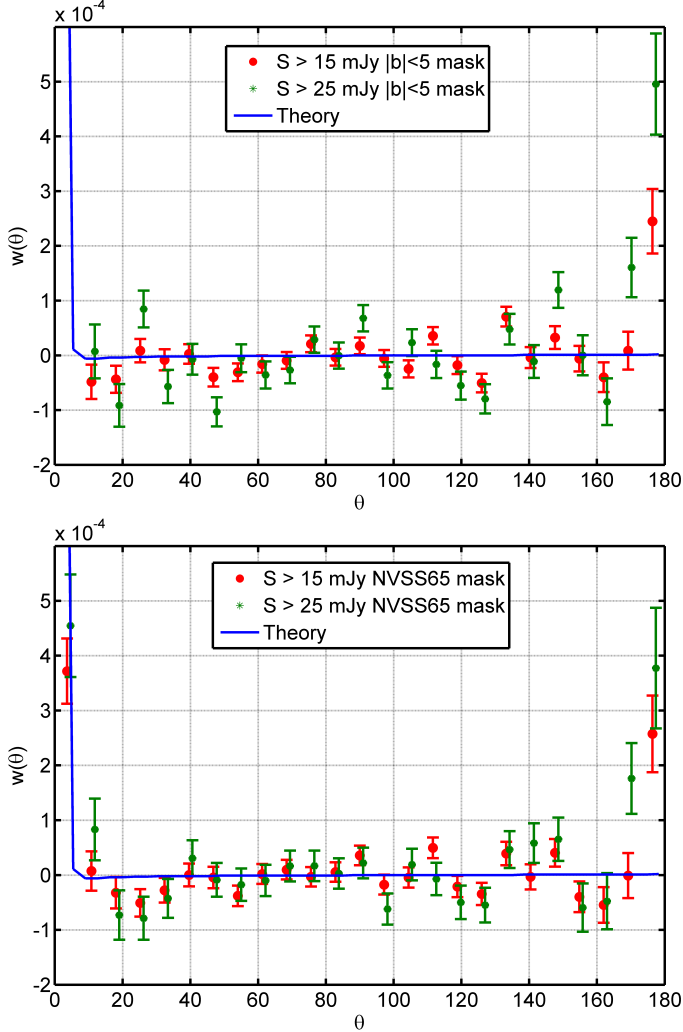


**Fig. 9.** Angular two-point correlation function  $w(\theta)$  from  $5^\circ$  galactic latitude cut (top panel) and the NVSS65 mask (bottom panel). In both cases we include a dipole correction.

$\theta \sim 90^\circ$ . Above that angular scale the data appear to be more noisy. Surprising are some quite large correlations at the largest angular scales close to  $180^\circ$ .

For angular scale between  $1^\circ$  and  $20^\circ$ , the 65% sky coverage guarantees that the  $w(\theta)$  estimator is averaged over a large number of independent sky patches. Artificial fluctuations caused by the survey or galactic foreground are suppressed in the average, and side lobes and multi-components source effects are expected to contaminate smaller angular scales (up to  $0.6^\circ$ ). In this range,  $w(\theta)$  is expected to be consistent with the theoretical prediction.

The result of an analysis at higher angular resolution for  $\theta < 20^\circ$  is shown in Fig. 10. In order to suppress the shot noise contribution we now focus on the  $S > 15$  mJy data set. We find that the NVSS65 mask improves the agreement with theoretical

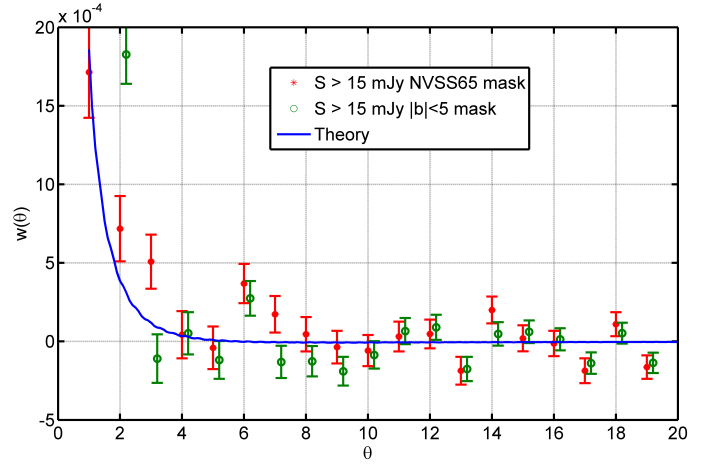


**Fig. 10.** Angular two-point correlation function at  $1^\circ < \theta < 20^\circ$  from the NVSS catalogue with dipole correction for two different masks.

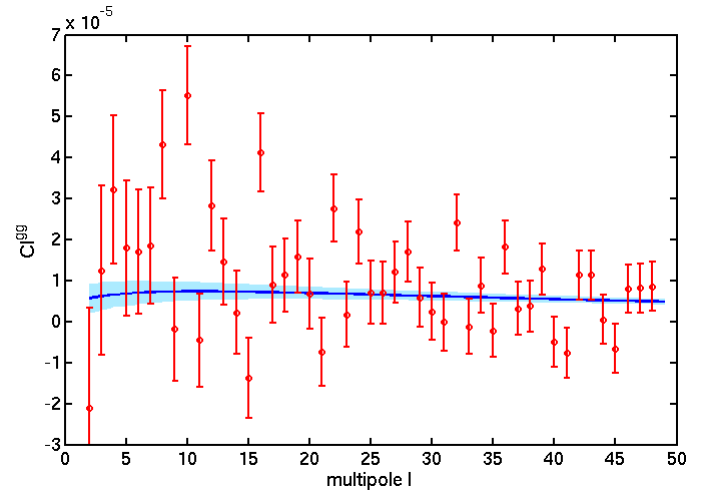


**Fig. 11.** NVSS angular power spectrum  $C_l$  for  $S > 15$  mJy, dipole corrected and NVSS65 mask.  $C_l$  is evaluated via a Legendre transformation from the angular two-point correlation function. The solid line and the band around it show the theoretical prediction and its cosmic variance.

predictions considerably. A discussion of the cosmological consequences is given below.

A complementary analysis to the angular two-point correlation function is to study the angular power spectrum. One way of measuring  $C_l$  is to do a Legendre transformation of the angular two-point correlation. The result of that transformation is shown in Fig. 11. The fact that many of the  $C_l$  turn out to have negative values shows that this measurement is quite noisy. Nevertheless, in the mean the  $C_l$  seem to agree well with the theoretical expectations, apart from a hand full of multipoles with even  $l$ , most prominently the  $l = 10$  mode.

## 5. Discussion

### 5.1. Cosmological implications

Let us now turn to the cosmological implications and a discussion of our findings in comparison with previous studies. In the following we focus on the results obtained by means of the NVSS65 mask, including the dipole correction as discussed above and a lower flux threshold of 15 mJy.



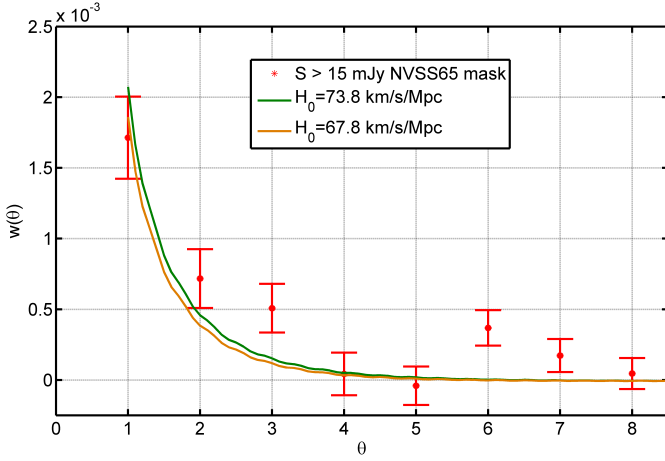


**Fig. 12.** Angular two-point correlation function as a test for the Hubble constant  $H_0$ . The measurement uses the NVSS65 mask with dipole correction.

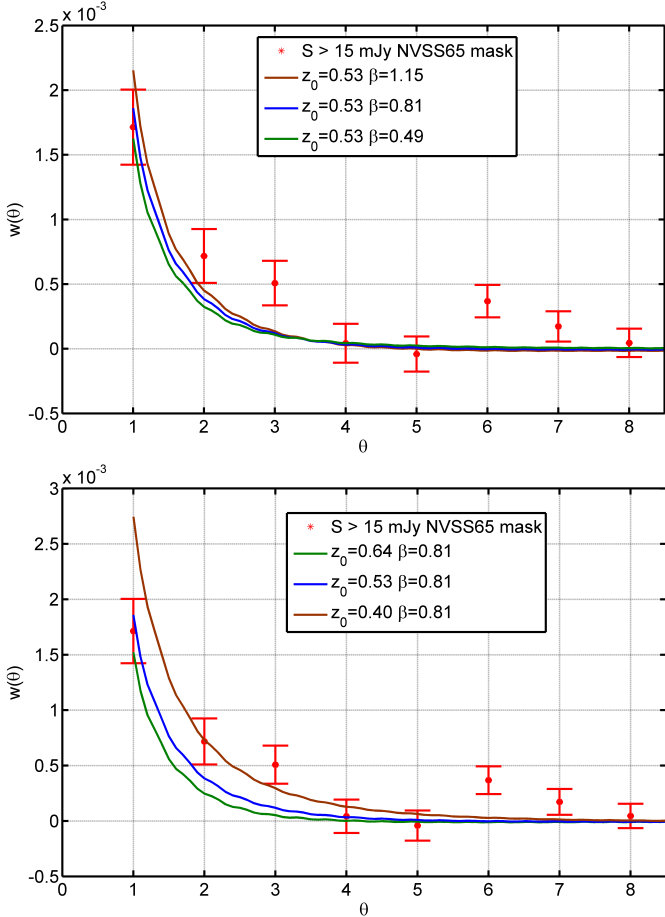


**Fig. 13.** Angular two-point correlation function for different redshift distributions.

A question of interest is the determination of the cosmological parameters of our minimal six-parameter cosmological standard model. For that purpose, the NVSS data alone cannot compete with high fidelity data from the CMB or from optical galaxy redshift surveys. Nevertheless it is interesting to investigate the consistency of the NVSS angular two-point correlation and angular power spectrum with the standard lore.

In Fig 12 we compare the NVSS angular two-point correlation with theoretical predictions at angular scales below  $9^\circ$  for different values of the Hubble constant  $H_0$ . The extreme values of  $H_0$  are disfavoured, and the Planck best-fit value of  $H_0 = 67.8$  km/s/Mpc provides also a good fit to NVSS data. Unfortunately, one can not use it to break the discrepancy with somewhat higher values from local measurements of  $H_0$ .

It is important to note, that the redshift distribution function also affects the NVSS angular two-point correlation at this angular scale. As shown in Fig 13, the parameter  $\beta$  modifies the slope of the two-point correlation, and the parameter  $z_0$  changes its slope and angular scale. Our angular two-point correlation measurement seems to prefer low  $z_0$  and  $\beta$ , which agrees with the results of Marcos-Caballero et al. (2013).

Putting those studies together we see a degeneracy of  $H_0$ ,  $z_0$  and  $\beta$ . The parameters of the bias factor  $b(z)$  do also participate in that degeneracy, which limits our ability to use today's radio continuum surveys for cosmological parameter estimation. However, it is an encouraging finding that the completely independent measurements of  $H_0$  (Planck),  $z_0$  and  $\beta$  (CENSORS) give rise to a picture that seems to be fully consistent with  $w(\theta)$  from NVSS.

The small angle two-point correlation is also an interesting probe of primordial non-Gaussianity. Previous results (Xia et al. 2010) claimed evidence for a primordial non-Gaussianity at the  $3\sigma$  level.  $w(\theta)$  is supposed to vanish at around  $4^\circ$  if the fluctuations are Gaussian, however their measurement of  $w(\theta)$  showed a constant shift from zero at  $1^\circ < \theta < 10^\circ$ , which they attributed to the effect of a primordial non-Gaussianity. However, adapting our procedure of dipole correction and optimal estimation of  $w(\theta)$ , we do not see such a shift. Our result thus fully agrees with primordial Gaussianity, as is shown in Fig. 10. To turn that into a precise new upper limit on  $f_{\text{nl}}$  is beyond the scope of this work.

Consistency with Gaussianity is also confirmed by the angular power spectrum shown in Fig. 11. A primordial non-Gaussianity would lead to an increase of angular power  $C_l$  at small multipoles (Xia et al. 2010; Desjacques & Seljak 2010). Our analysis shows no evidence for such an increase. Note that this contradicts the previous results from Blake et al. (2004) and Marcos-Caballero et al. (2013). We tried to understand what is responsible for the removal of the apparent non-Gaussianity, but it turns out that it is impossible to attribute it to a single effect. The dipole changes the low  $l$  multipoles as one reconstructs the multipole moments from an incomplete sky, but we verified that the dipole effect alone is not large enough. We also use a slightly higher threshold (15 instead of 10 mJy) in our analysis, which also reduces the direction dependent effects in the NVSS catalogue (see table 1). The masking of regions around bright sources appears not to influence the analysis on the largest scales. On the other hand, using the Landy-Szalay estimator compared to suboptimal methods seems to be important. We conclude that the sum of our studies of the systematics of the NVSS catalogue is essential and allows us to get rid of a spurious non-Gaussianity.

## 5.2. Residual systematics

The theoretical prediction based on the  $\Lambda$ CDM model suggested  $C_l \approx 5 \times 10^{-6}$ . Our measurements agree rather well with that prediction, with some exceptions. The quadrupole cannot be detected at any significant level and the power at  $l = 10$  is an order of magnitude larger than expected. However, at larger  $l$ , up to  $l \sim 60$ , the  $C_l$  are consistent with the theoretical prediction, which is in agreement with previous analysis of the ISW effect

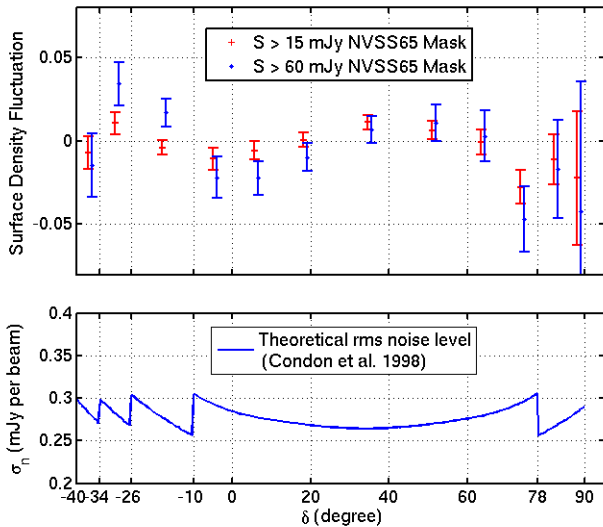


**Fig. 14.** Top panel: Surface density fluctuation ( $\Delta\sigma/\bar{\sigma}$ ) of NVSS sources at  $S > 60$  mJy and  $S > 15$  mJy after applying the NVSS65 mask. Bottom panel: The theoretical rms noise level of the NVSS catalogue from Condon et al. (1998). The VLA geodetic latitude is  $34^{\circ}04'44''$ .

Hernández-Montegudo (2010). Higher multipole moments are noisy and statistically consistent with zero.

Let us finally discuss the angular scales at  $\theta > 20^{\circ}$  and look in more detail at the corresponding multipole moments up to  $l = 10$ . For a simple galactic isolatitude cut, we found significantly more power at low multipole moments, with  $l = 4$  being the dominant mode (not shown here). The essential step to get rid of this extra power is to take into account direction dependent systematic effects in the NVSS catalogue. Our NVSS65 mask allows us to reduce the  $l = 4$  mode and to recover an overall flat angular power spectrum. However, even with the NVSS65 mask, some of the  $C_l$ s are one order of magnitude larger than the prediction at  $l < 10$ . One of the reason could be due to remaining surface density fluctuations at different declinations.

We find a clear anti-correlation between the surface density and the theoretical rms noise of the NVSS catalog, Fig. 14. The declination dependence of the theoretical rms noise fluctuations at  $-40^{\circ} < \delta < -10^{\circ}$  is due to changes in the snapshot integration time. When the VLA points to the horizon, the effect of the projection of the uv plane, combined with ground and ionospheric noise, decreases the effective signal to noise ratio of the survey. As can be seen in Fig. 14 this effect is not limited to the faintest sources, but is also there for brighter sources at  $S > 60$  mJy. Thus only the most extreme influence of the direction dependent systematics can be cured by means of a lower flux threshold.

To further probe whether these direction dependent effects affect the low- $l$  multipoles, we investigated the angular pseudo-power spectrum, which are obtained through a decomposition into spherical harmonics on the pixelized galaxy number count. For this we used HEALPIX. In figure 15 we show estimates of the pseudo- $C_l$  for two different normalizations. In the first case, we normalize the pixel count with the mean pixel count of the full survey  $\bar{n}$ , i.e.

$$x_i = \frac{n_i - \bar{n}}{\bar{n}}. \quad (18)$$

The second case is motivated by Vielva et al. (2006). We divide the map along the declination, based on durations of the snap-

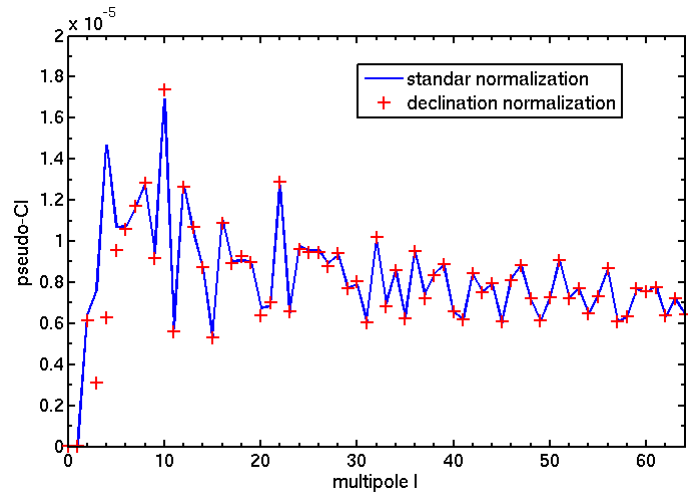


**Fig. 15.** The HEALPIX pseudo- $C_l$  of NVSS catalog for  $S > 15$  mJy and radio dipole subtracted.

shots, and subtract the mean pixel count  $\bar{n}_{\delta_i}$  at declination  $\delta_i$ ,

$$x_i = \frac{n_i - \bar{n}_{\delta_i}}{\bar{n}}. \quad (19)$$

The latter procedure was also used in the Planck analysis of the ISW effect (Planck Collaboration. XIX. 2014; Planck Collaboration. XXI. 2015).

The second procedure, erases the source density fluctuations along the declination direction. As can be seen in Fig. 15, the  $l = 3, 4, 5$  multipoles are significantly reduced by the declination mean subtraction, which strongly implies that the  $l = 4$  mode fluctuation are caused by the direction dependent noise of the NVSS catalogue. On the other hand, the large  $l = 10$  mode is not affected by that normalization at all and it remains unclear why it exceeds the expectation by an order of magnitude. Using this declination normalisation for a cosmological analysis like in (Vielva et al. 2006; Planck Collaboration. XIX. 2014) certainly suppresses fluctuations on large scales, but the procedure cannot distinguish direction dependent effects from real fluctuations and it is very hard to assign an error estimate to it.

Before concluding, let us mention a curious observation. Looking carefully at Fig. 11, we observe a parity asymmetry in the  $C_l$ : the power of even multipoles  $l = 4, 8, 10, 12, 16, 22, 24, 32, \dots$  is higher than that of their odd neighbors. This even parity preference can also be seen from the fact that  $w(180^{\circ}) > 0$ . A similar effect was observed in the CMB angular power spectrum, where the parity asymmetry is the opposite Kim & Naselsky (2010). There the odd  $l(l+1)C_l/2\pi s$  are larger than the even ones. However, this suggests that the two parity asymmetries do not share the same origin, if both of them are real.

## 6. Conclusion

In this paper we revisited the angular two-point correlation function  $w(\theta)$  and angular power spectrum  $C_l$  from the NVSS catalogue of radio galaxies. The focus of our work was to investigate systematic effects in the NVSS catalogue. In order to minimize the contribution of these effects in the cosmological analysis, we provide a new NVSS mask with 64.7% percent of sky, called NVSS65. We also find that it is essential to account for the radio dipole and to use a lower flux threshold. We found that our mask

significantly improves the  $\chi^2$  value of the angular two-point correlation function on all angular scales.

For angular scales between 1 and 20 degrees,  $w(\theta)$  agrees with the flat  $\Lambda$ CDM model without introducing primordial non-Gaussianity.

Thus we have shown that to fully explore the cosmological potential of continuum radio surveys, one has to understand and investigate the systematic effects related with flux calibration, especially direction dependent effects of the calibration. Besides, the effect of the cosmic radio dipole affects the reconstruction of higher multipole moments and the attempts to measure or constrain primordial non-Gaussianity.

To obtain an improved upper limit on  $f_{\text{nl}}$  or to constrain other cosmological parameters at a redshift of about unity is beyond the scope of this work, as it would need an extensive study of the uncertainties coming from our understanding of the density, luminosity and bias evolution of radio galaxies. However, our analysis shows, that the radio sky is in remarkable good agreement with the standard model of cosmology after Planck. It will also be interesting to improve the ISW analysis of the Planck-NVSS cross correlation by means of the new NVSS65 mask and including a radio dipole correction, as well as a higher flux threshold.

Our results further suggest that  $w(\theta)$  from full sky radio continuum surveys can be used to constrain cosmological parameters at an epoch that is hardly accessible to other probes. Planned and upcoming surveys with instruments like LOFAR, ASKAP, MeerKAT and eventually SKA will allow us to reduce the shot noise, increase angular resolution and sensitivity, while covering all sky, extend the studies to several frequency bands (all of our discussion here is limited to 1.4 GHz) and improve the control of systematic effects. For more details see Raccanelli et al. (2012) and Jarvis et al. (2015) and references therein.

*Acknowledgements.* We thank Anne-Sophie Balleier, Daniel Boriero, Bin Hu, Dragan Huterer, Hans-Rainer Klöckner, Alvise Raccanelli, and Matthias Rubart for valuable comments and discussions. We acknowledge financial support from Deutsche Forschungsgemeinschaft (DFG) via the Research Training Group “Models of Gravity” (RTG 1620). We are grateful for the possibility to perform the numerical computations on the Nordrhein-Westfalen state computing cluster at RWTH Aachen. We acknowledge the use of the NVSS catalogue Condon et al. (1998), provided by the NRAO. This work made extensive use of the HEALPIX Gorski et al. (2005) and the CLASS Lesgourgues & Tram (2011); Di Dio et al. (2013) packages.

## References

- Blake, C., Ferreira, P. G., & Borrill, J. 2004, MNRAS, 351, 923  
 Blake, C. & Wall, J. 2002a, Nature, 416, 150  
 Blake, C. & Wall, J. 2002b, MNRAS, 329, L37  
 Brookes, M., Best, P., Peacock, J., Rottgering, H., & Dunlop, J. 2008, MNRAS, 385, 1297  
 Chen, S. & Schwarz, D. J. 2015, Phys. Rev. D, 91, 043507  
 Condon, J. J., Cotton, W. D., Greisen, E. W., et al. 1998, ApJ, 115, 1693  
 Copi, C. J., Huterer, D., Schwarz, D. J., & Starkman, G. D. 2015, MNRAS, 449, 3458  
 Dalal, N., Doré, O., Huterer, D., & Shirokov, A. 2008, Phys. Rev. D, 77, 123514  
 de Zotti, G., Massardi, M., Negrello, M., & Wall, J. 2010, A&A Rev., 18, 1  
 Desjacques, V. & Seljak, U. 2010, Classical and Quantum Gravity, 27, 124011  
 Di Dio, E., Montanari, F., Lesgourgues, J., & Durrer, R. 2013, J. Cosmology Astropart. Phys., 1311, 044  
 Ellis, G. F. R. & Baldwin, J. E. 1984, MNRAS, 206, 377  
 Gibelyou, C. & Huterer, D. 2012, MNRAS, 427, 1994  
 Gorski, K., Hivon, E., Banday, A., et al. 2005, ApJ, 622, 759  
 Hernández-Monteagudo, C. 2010, A&A, 520, A101  
 Ho, S., Hirata, C., Padmanabhan, N., Seljak, U., & Bahcall, N. 2008, Phys. Rev. D, 78, 043519  
 Hoaglin, D. C. & Tukey, J. W. 2006, Exploring Data Tables, Trends, and Shapes (John Wiley & Sons, Inc)  
 Jarosik, N., Bennett, C., Dunkley, J., et al. 2011, ApJS, 192, 14  
 Jarvis, M., Bacon, D., Blake, C., et al. 2015, PoS, AASKA14, 018

- Kim, J. & Naselsky, P. 2010, ApJ, 714, L265  
 Landy, S. D. & Szalay, A. S. 1993, ApJ, 412, 64  
 Lesgourgues, J. & Tram, T. 2011, J. Cosmology Astropart. Phys., 1109, 032  
 Maartens, R., Zhao, G.-B., Bacon, D., Koyama, K., & Raccanelli, A. 2013, J. Cosmology Astropart. Phys., 1302, 044  
 Marcos-Caballero, A., Vielva, P., Martínez-González, E., et al. 2013, ArXiv e-prints 1312.0530  
 Matarrese, S., Verde, L., & Jimenez, R. 2000, ApJ, 541, 10  
 Naselsky, P., Zhao, W., Kim, J., & Chen, S. 2012, ApJ, 749, 31  
 Peebles, P. 1980, The Large-Scale Structure of the Universe (Princeton Univ. Press)  
 Planck Collaboration. XIX. 2014, A&A, 571, A19  
 Planck Collaboration. XVI. 2014, A&A, 571, A16  
 Planck Collaboration. XVI. 2015, ArXiv e-prints 1506.07135  
 Planck Collaboration. XXI. 2015, ArXiv e-prints 1502.01595  
 Planck Collaboration. XXVII. 2014, A&A, 571, A27  
 Raccanelli, A., Zhao, G.-B., Bacon, D. J., et al. 2012, MNRAS, 424, 801  
 Rubart, M. 2015, PhD thesis, University Bielefeld  
 Rubart, M., Bacon, D., & Schwarz, D. J. 2014, A&A, 565, A111  
 Rubart, M. & Schwarz, D. J. 2013, A&A, 555, A117  
 Schwarz, D. J., Starkman, G. D., Huterer, D., & Copi, C. J. 2004, Phys.Rev.Lett., 93, 221301  
 Singal, A. K. 2011, ApJ, 742, L23  
 Vielva, P., Martínez-González, E., & Tucci, M. 2006, MNRAS, 365, 891  
 Xia, J.-Q., Viel, M., Baccigalupi, C., et al. 2010, ApJ, 717, L17  
 Yoho, A., Aiola, S., Copi, C. J., Kosowsky, A., & Starkman, G. D. 2015, Phys.Rev., D91, 123504